Passive Dynamic Biped Walking—Part I: Development and Validation of an Advanced Model

Derek Koop

Christine Q. Wu

Department of Mechanical Engineering,
University of Manitoba,
Winnipeg, MB R3T 5V6, Canada

Passive dynamic walking is a manner of walking developed, partially or in whole, by the energy provided by gravity. Studying passive dynamic walking provides insight into human walking and is an invaluable tool for designing energy-efficient biped robots. The objective of this research was to develop a continuous mathematical model of passive dynamic walking, in which the Hunt–Crossley contact model, and the LuGre friction model were used to represent the normal and tangential ground reactions continuously. A physical passive walker was built to validate the proposed mathematical model. A traditional impact-based passive walking model was also used as a reference to demonstrate the advancement of the proposed passive dynamic walking model. The simulated gait of the proposed model matched the gait of the physical passive walker exceptionally well, both in trend and magnitude. [DOI: 10.1115/1.4023934]

1 Introduction

Passive dynamic walking is a manner of walking that is driven by gravitational potential energy of the legs and the body. Studying passive dynamic biped walking helps create an understanding of how gravity affects the biped gait and is useful in two main areas: the development of humanoid robotics and understanding the human gait. The two main goals for producing a biped robot gait are energy efficiency and dynamic balance. Fully passive dynamic biped walkers are very energy-efficient, using only the energy provided by gravity to walk down a shallow slope. However, passive dynamic biped walkers are inherently unstable. Understanding what affects the robustness of a passive walker may provide insights into how to control biped robots to maintain postural balance while maintaining an energy-efficient gait. Humans use the gravitational potential energy of the body to help develop their gait along with their muscle energy. This type of gait is often referred to as a semipassive dynamic gait. Understanding how the mechanics of the legs shape the gait can provide insight into how humans develop their gait.

Studying anthropomorphic passive dynamic walking machines started in the 1980s with Tad McGeer, who was inspired by earlier research completed by Mochon and McMahon [1]. McGeer [2,3] examined the passive gait through the use of mathematical models and experimental walking machines. Following McGeer's initial research, Goswami et al. [4,5] and Garcia et al. [6] studied the stability of a two-link passive walker using an impact-based model. Research of passive dynamic walking can be categorized into two main groups: experimental studies and analysis through mathematical modeling, with a majority belonging to the latter.

Mathematical modeling is an excellent tool for analyzing passive dynamic walking. A number of passive dynamic walking models can been found in the literature, ranging from a two-link passive walker [2,5], a three link passive walker [7], to a five-link passive walker with an upper body [8]. In Ref. [9], an impact model for a kinematic chain, in a series formation, was derived. These types of passive dynamic walking models, referred to as impact-based models in this paper, are discontinuous and rely on a number of assumptions. A majority of impact-based passive walking models rely on the assumptions that the heel strike impacts are instantaneous and plastic and no sliding occurs during impact. These assumptions may create artificial gaits that are not representative of reality. In the aforementioned mathematical models, [2,5,7,8], the stance foot was assumed to be in pure rolling with the friction between the foot and the ground modeled using discontinuous friction models or neglected all together. The addition of friction between the ground contacts can change the resulting gait of a passive walking model noticeably and reduces the likelihood of producing artificial gaits [2]. An additional concern with the traditional impact model, raised in Ref. [10], is the determination of phase after the impact, where the phase could be single support, double support, or support sliding.

One theoretical concern of having discontinuous dynamic models of passive walking, due to the simplified impact models and friction models, is that the differential equations contain discontinuous terms. The discontinuous terms cause the dynamic systems to be nonsmooth, which violates the fundamental requirements of the conventional solution theories to ordinary differential equations (i.e., the vector fields must be at least Lipschitz continuous). Thus, there is no guarantee as to the existence and uniqueness of the solution. Furthermore, with respect to classical solution theories, one cannot even define a solution, much less discuss its existence and uniqueness and obtain the solution [11].

More recently, passive walking models that use continuous force-based contact models and friction models to describe the ground reaction forces have been developed. Normal force and friction force modeling is the key to simulating a realistic passive walking gait. A review of contact modeling is provided in Ref. [12], and a review of friction modeling is provided in Ref. [13]. An advantage of the force-based method is that multiple contacts (double support phase) are easily incorporated. In spite of the advantages, for a contact model to be valid, the model needs to be compared to experimental measurements, like the validation case given in Ref. [14]. Force-based passive walking models were presented in Refs. [15–18]. The effects of the contact model parameters on the gait were examined in Ref. [15], and the effects of compliance in the passive walker structure were studied in Ref. [16]. Research has also been carried out to compare the impact model and force-based contact models [19]. A comprehensive analysis of common compliant contact force models was recently presented in Ref. [20]. The models presented in Refs. [15] and [16] used friction models from dynamic modeling software.

Contributed by the Design Engineering Division of ASME for publication in the Journal of Computational and Nonlinear Dynamics. Manuscript received December 11, 2012; final manuscript received February 28, 2013; published online April 19, 2013. Assoc. Editor: Parviz Nikravesh.

The limitation of the respective friction models is that they apply a smaller force as the sliding velocity between the two surfaces tends toward zero and do not apply a force at a zero sliding velocity (i.e., a completely static friction force cannot be achieved).

To determine if the assumptions used to derive a passive dynamic walking model are valid, the model must be compared against a physical passive walker. In McGeer's initial work [2], a preliminary comparison between simulations of passive walking and an experimental passive gait were completed. In Ref. [2], the leg angle[1] of the simulated passive walker was in agreement with the physical passive walker experiments when the simulations accounted for rolling friction. However, the step period of the simulations was unable to match the physical experiments. Following McGeer's work, there have been very limited results on validating mathematical models against experimental passive dynamic walker data. Two reasons why it is difficult to compare: (1) a majority of passive walking models do not produce realistic friction and normal contact forces and (2) lack of experimental gait measurements of passive dynamic biped walkers.

Experimental results of passive dynamic walking are vital for validating mathematical models. There are some published works that provide gait measurements of passive dynamic walkers. In Refs. [21] and [22], gait measurements were taken with the use of a video camera. Trends of the step length and walking speed were found, but the trend of the step period was not found, due to the measurement frequency. In Ref. [23], experimental analysis of a kneed biped walker using an encoder and an accelerometer to measure the gait parameters is provided. The frequency of the measurements was high enough to capture a clear trend of the step period. An experimental two-link passive biped was tested to measure the robustness of a passive walker in Ref. [24].

A new mathematical model of passive dynamic walking is presented in this paper that models the contact and friction forces continuously. Compared to the traditional impact-based passive walking model, the proposed mathematical model is able to additionally model the double support phase, along with the single support phase, and heel strike event. The double support phase, in the case of a two-link walker, is due to the sliding or deformation of the contacts. To model the contact events, the continuous Hunt–Crossley contact model and the LuGre friction model were incorporated in the proposed passive walking model. To validate the proposed passive walking model, a physical passive walker was designed and built. The resulting gait of both the physical passive walker and the proposed passive walking model were compared to determine the validity of the proposed passive walking model.

2 Mathematical Modeling

The proposed passive walking model consists of two links, each with distributed mass and arced foot. The passive walking model also has a nonrotating mass located at the hip. The hip mass simulates the effects of an upper body. The proposed passive walking model is described by one unified set of continuous ordinary differential equations that describes the entire motion of the passive walker. The proposed passive walking model is able to capture single support and double support dynamics, with the addition of the friction and normal force contact models. The friction between the foot and ground is described by the LuGre friction model. The normal contact forces between the foot and the ground are described by the Hunt–Crossley model. The friction at the hip joint is neglected.

Figure 1 shows a schematic of the passive walking mathematical model, where l is the length of the legs, b is the distance of the leg center of mass from the hip, and ρ is the foot radius. The parameter δ is the angle offset of the foot. Each leg has a distributed mass m and a radius of gyration of r_g with respect to the center of mass. The hip joint of the passive walker is located by the two

[1]Angle between the legs at the instance of heel strike.

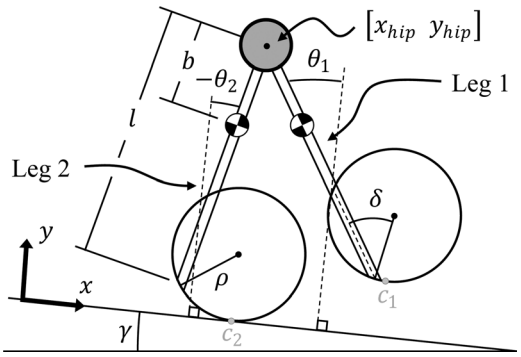

Fig. 1 Model diagram

coordinates x_{hip} and y_{hip}. There is a nonrotating mass, denoted by M, located at the hip. The angle of each leg, with reference to the normal of the ramp, is denoted by θ_1 and θ_2. The ramp is at an inclination γ. The reference frame is rotated so that the x-axis is in line with the direction of the ramp. There are two points, c_1 and c_2, marked on the feet, which are the contact points or impending contact points. The points c_1 and c_2 are the points on the feet with the lowest y coordinate.

The equations of motion, Eq. (1), are derived using Lagrangian mechanics, where the matrix $\boldsymbol{q}$ describes the state of the system, $\boldsymbol{M}(\boldsymbol{q})$ is the mass matrix, $\boldsymbol{H}(\boldsymbol{q},\dot{\boldsymbol{q}})$ is the centripetal and Coriolis forces, $\boldsymbol{G}(\boldsymbol{q})$ is the gravitational force, and $\boldsymbol{F}(\boldsymbol{q},\dot{\boldsymbol{q}})$ are the generalized external forces on the system.

$$\boldsymbol{M}(\boldsymbol{q})\ddot{\boldsymbol{q}} + \boldsymbol{H}(\boldsymbol{q},\dot{\boldsymbol{q}}) + \boldsymbol{G}(\boldsymbol{q}) = \boldsymbol{F}(\boldsymbol{q},\dot{\boldsymbol{q}}) \tag{1}$$

$$\boldsymbol{q} = \begin{bmatrix} x_{hip} \\ y_{hip} \\ \theta_1 \\ \theta_2 \end{bmatrix}, \quad \dot{\boldsymbol{q}} = \begin{bmatrix} \dot{x}_{hip} \\ \dot{y}_{hip} \\ \dot{\theta}_1 \\ \dot{\theta}_2 \end{bmatrix}, \quad \ddot{\boldsymbol{q}} = \begin{bmatrix} \ddot{x}_{hip} \\ \ddot{y}_{hip} \\ \ddot{\theta}_1 \\ \ddot{\theta}_2 \end{bmatrix} \tag{2}$$

$$\boldsymbol{M}(\boldsymbol{q}) = \begin{bmatrix} M+2m & 0 & mb\cos\theta_1 & mb\cos\theta_2 \\ 0 & M+2m & mb\sin\theta_1 & mb\sin\theta_2 \\ mb\cos\theta_1 & mb\sin\theta_1 & mb^2+r_g^2 & 0 \\ mb\cos\theta_2 & mb\sin\theta_2 & 0 & mb^2+r_g^2 \end{bmatrix} \tag{3}$$

$$\boldsymbol{H}(\boldsymbol{q},\dot{\boldsymbol{q}}) = \begin{bmatrix} -mb\dot{\theta}_1^2\sin\theta_1 - mb\dot{\theta}_2^2\sin\theta_2 \\ -mb\dot{\theta}_1^2\cos\theta_1 + mb\dot{\theta}_2^2\cos\theta_2 \\ 0 \\ 0 \end{bmatrix} \tag{4}$$

$$\boldsymbol{G}(\boldsymbol{q}) = g\begin{bmatrix} -(M+2m)\sin\gamma \\ (M+2m)\cos\gamma \\ mb\sin(\theta_1-\gamma) \\ mb\sin(\theta_2-\gamma) \end{bmatrix} \tag{5}$$

$$\boldsymbol{F}(\boldsymbol{q},\dot{\boldsymbol{q}}) = \begin{bmatrix} F_{f_1}+F_{f_2} \\ F_{N_1}+F_{N_2} \\ F_{f_1}c_{y_1}^{\text{hip}} + F_{N_1}c_{x_1}^{\text{hip}} \\ F_{f_2}c_{y_2}^{\text{hip}} + F_{N_2}c_{x_2}^{\text{hip}} \end{bmatrix} \tag{6}$$

The normal force applied on each foot is denoted by F_{N_1} and F_{N_2}. The friction force between each foot and the ground are denoted by F_{f_1} and F_{f_2}. The position of the contact points, shown in Fig. 1 relative to the hip, is described by the vector $\vec{c}_i^{\,\text{hip}}$.

$$\vec{c}_i^{\,\text{hip}} = [l\sin\theta_i - \rho\sin(\theta_i-\delta)\ \ l\cos\theta_i - \rho(\cos(\theta_i-\delta)-1)] \tag{7}$$

The global position of the contact points of the two feet are defined by $\left(\vec{c}_i\right)$, and their corresponding velocities are defined by $\left(\dot{\vec{c}}_i\right)$.

$$\vec{c}_i = \left[x + l\sin\theta_i - \rho\sin(\theta_i - \delta)\ \ y - l\cos\theta_i + \rho(\cos(\theta_i - \delta) - 1)\right] \tag{8}$$

$$\dot{\vec{c}}_i = \left[\dot{x} + \dot{\theta}_i(l\cos\theta_i - \rho\cos(\theta_i - \delta) + \rho)\ \dot{y} - \dot{\theta}_i(l\sin\theta_i + \rho\sin(\theta_i - \delta))\right] \tag{9}$$

2.1 Contact Model. The Hunt–Crossley contact model [25] is an extension of the Hertz contact model [26] to include hysteretic damping in the contact forces. For dynamic simulations, the contact force is described by the interpenetration, h, and the interpenetration velocity, $\dot{h}$, of the two bodies. The interpenetration and corresponding velocities are described by Eqs. (10) and (11), respectively. Figure 2 shows a schematic of the interpenetration of the two bodies.

$$h_i = \begin{cases} 0 & \text{for} \quad c_{y_i} \geq 0 \\ -c_{y_i} & \text{for} \quad c_{y_i} < 0 \end{cases} \tag{10}$$

$$\dot{h}_i = \begin{cases} 0 & \text{for} \quad c_{y_i} \geq 0 \\ -\dot{c}_{y_i} & \text{for} \quad c_{y_i} < 0 \end{cases} \tag{11}$$

The level of the normal force (N_i) is determined by Eq. (12), where n, p, and q are dependent on the geometry of the contact and the material of the two bodies. For the passive dynamic walking model, $n = p = 3/2$ and $q = 1$, which corresponds to a spherical or cylindrical contact.

$$N_i - k_s h_i^n + k_d h_i^p h_i^q \tag{12}$$

The normal force, F_{N_i}, is equal to the level of force if the level of the force is greater than or equal to zero. With the definition of the interpenetration, the two bodies are assumed to be in contact if $h > 0$, which can lead to a negative force in Eq. (12) if the restitution velocity is great enough. Equation (13) is introduced to account for this. In reality, this situation would occur when separation of the two bodies occurs before both bodies have restored to their undeformed shape. Due to the fact that N_i approaches zero in a continuous manner, the system solution remains continuous with the introduction of the condition F_{N_i}.

$$F_{N_i} = \begin{cases} N_i & \text{for} \quad N_i \geq 0 \\ 0 & \text{for} \quad N_i < 0 \end{cases} \tag{13}$$

The advantage of using a force-based contact model, like the Hunt–Crossley model, is that there is no discontinuity at the heel strike event. The Hunt–Crossley model can also simulate multiple contact dynamics, which is important for biped walking to simulate the double support phase.

2.2 Friction Model. The friction between the foot and the surface is modeled using the LuGre friction model [27]. The LuGre friction model is a continuous dynamic model that can describe the static friction force, Coulomb friction force, and the transition between the two. The LuGre model can be visualized as two sets of elastic bristles, as shown in Fig. 3, where z is the bristle deflection. The friction force determined by the LuGre friction model is given by Eq. (14), where the terms that describe the viscous friction are omitted.

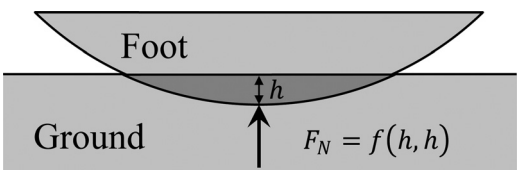

Fig. 2 Schematics of interpenetration of two bodies

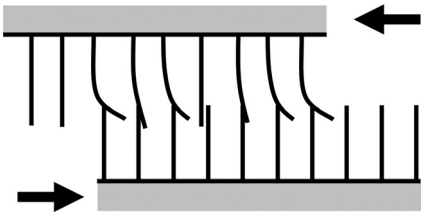

Fig. 3 Visualization of the LuGre model

$$F_{f_i} = -(\sigma_0 z_i + \sigma_1 \dot{z}_i) F_{N_i} \tag{14}$$

$$\dot{z}_i = v_i - \sigma_0 \frac{[v_i]}{g_L(v_i)} z_i \tag{15}$$

$$g_L(v_i) = \mu_c + (\mu_s - \mu_c) e^{-\left(\frac{v_i}{v_s}\right)^2} \tag{16}$$

The subscript $i = 1$ or 2 corresponds to each foot. The sliding velocity between the two surfaces, v_i, is represented by $\dot{c}_{x_i}$ in the passive walking model.

$$\dot{c}_{x_i} = \dot{x} + \dot{\theta}_i(l\cos\theta_i - \rho\cos(\theta_i - \delta) + \rho) \tag{17}$$

The variables σ_0 and σ_1 control the stiffness and damping of the bristle deflection, respectively. The static and Coulomb friction coefficients are represented by μ_s and μ_c, respectively. The Stribeck velocity is represented by v_s. Increasing the sliding velocity from zero, the Stribeck velocity is the initial point that the friction force begins to decrease with increasing sliding velocity.

2.3 State Space Model Swing Leg Ground Clearance. In order to solve the mathematical model, the equations are transformed into a state space representation. The state space model is formed from incorporating the friction state observers, Eq. (15), and the contact force equations, Eqs. (13) and (14), with the equations of the motion, Eq. (1). The final state space model, Eq. (18), has ten states that are described in Eq. (19). The whole set of equations of the state space can be found in Appendix A.

$$\dot{\boldsymbol{Q}} = f(\boldsymbol{Q}) \tag{18}$$

$$\boldsymbol{Q} = [Q_1\ Q_2\ Q_3\ Q_4\ Q_5\ Q_6\ Q_7\ Q_8\ Q_9\ Q_{10}]^T = \left[x_{\text{hip}}\ y_{\text{hip}}\ \theta_1\ \theta_2\ \dot{x}_{\text{hip}}\ \dot{y}_{\text{hip}}\ \dot{\theta}_1\ \dot{\theta}_2\ z_1\ z_2\right] \tag{19}$$

In spite of continuous contact and friction force models, the equations of the passive walking model, Eq. (18), are stiff, due to the high rates of acceleration at the heel strike event. The detection of the precise instant of contact is one of the most important challenging parts in simulating multibody systems with contact interactions [28]. In general, standard numerical solvers for ordinary differential equations (ODEs) are numerically unstable when solving stiff equations, unless a very small step size is chosen. Sometimes, this small step size is beyond double precision and becomes unpractical. The solution to Eq. (18) was approximated using ODE15S in Matlab, which is designed for solving stiff equations. A detailed description of ODE15S can be found in Ref. [29]. The maximum time step for the solution was set to 10^{-4}. When the swing leg would come in contact with the ground, the time step would typically decrease to the order of 10^{-6} to satisfy the error tolerance.

Unlike biped walkers with knees, two-link biped walkers need a mechanism for the swing leg to clear the ground. In physical experiments, this ground clearance can be created with "stepping stones." In the numerical simulations, the effect of stepping stones is established by switching between two support phases: single support and double support. The two support phases are represented by Double Support = True or False. In the single support

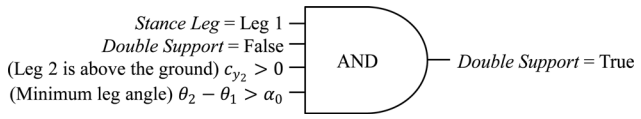

Fig. 4 Transition to double support phase when Leg 1 is the stance leg

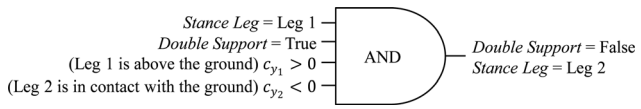

Fig. 5 Transition to single support phase to single support on Leg 2

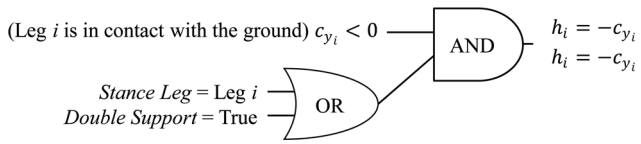

Fig. 6 Determining the interpenetration value for Leg *i*

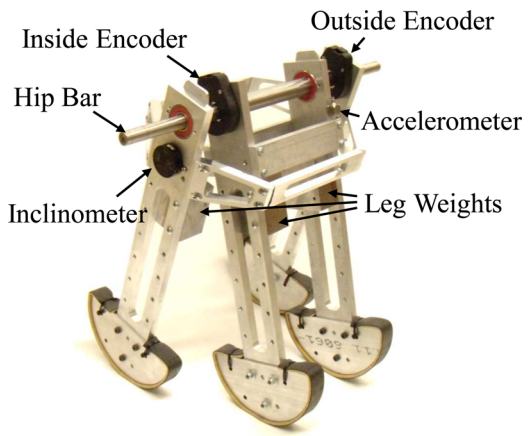

Fig. 7 Picture of HM2L with features labeled

phase (Double Support = False), one leg is the stance leg and the other the swing leg. The leg that is the swing leg can penetrate the ground without incurring reaction forces. The initial conditions are chosen so that the walker is just starting the swing phase of the next step; therefore, Double Support = False and Stance Leg = Leg 1 if $\theta_1 > \theta_2$ or Stance Leg = Leg 2 if $\theta_2 > \theta_1$.

During the simulation, at every time step, the program checks if the system has transitioned to another phase. The transition to double support is determined by the condition in Fig. 4, and the transition to single support is determined by the condition in Fig. 5. The parameter c_y is the y-coordinate of the contact point, and α_0 is the minimum inner leg angle.

Once the support phase and stance leg are determined, the value of the penetration, h, and penetration velocity, $\dot{h}$, are determined. Initially, the penetration and penetration velocity are set to zero and are only changed if the condition in Fig. 6 is met.

3 Validation of the Proposed Model

To validate the model presented in Sec. 2, an experimental passive walking machine, named Hip Mass 2 Links (HM2L), was built. This section presents the design of the experimental passive walker, gait measurement system, and the test platform.

3.1 Overview of Physical Passive Walker and Gait Measurement Sensors. The experimental passive biped walker, HM2L, is shown in Fig. 7. HM2L consists of two links with arced feet and a hip mass. The hip mass can rotate independently from the two legs. HM2L has no means for swing foot clearance, so the biped walker must walk on "stepping stones," as shown in Fig. 8. To measure the gait parameters of the experimental passive biped walker, the design for HM2L incorporated two optical rotary encoders to measure the relative rotation between each leg, a single inclinometer to determine global orientation, and an accelerometer to detect the instance of heel strike.

The legs of the experimental walker are connected to the hip via roller bearings. To limit the motion of the passive walker to the sagittal plane, the inside leg pair and outside leg pair are coupled together. Table 1 provides the geometric parameters of the experimental walker. HM2L also has four movable leg weights, shown in Fig. 7. The leg weights consist of ~45% of the walker's total mass and can be moved to six discrete locations. Table 2 provides the mass parameters of the experimental walker, and Table 3 provides the center of mass and radius of gyration for each mass location. The test ramp, partially shown in Fig. 8, is 9.75 m long and 0.86 m wide.

The two optical rotary encoders for measuring the inner leg angle have a 0.05 deg resolution. Each encoder provides the relative angle between the corresponding leg set and the hip bar. A Kistler Miniature PiezoBeam Triaxial accelerometer with a range of ±50 g was attached to the walker on the position labeled in Fig. 7. This location was chosen so that the accelerometer would be protected from damage and also so the data cable would have a minimal effect on the gait. A US Digital X3M absolute inclinometer was used to determine the global orientation of the

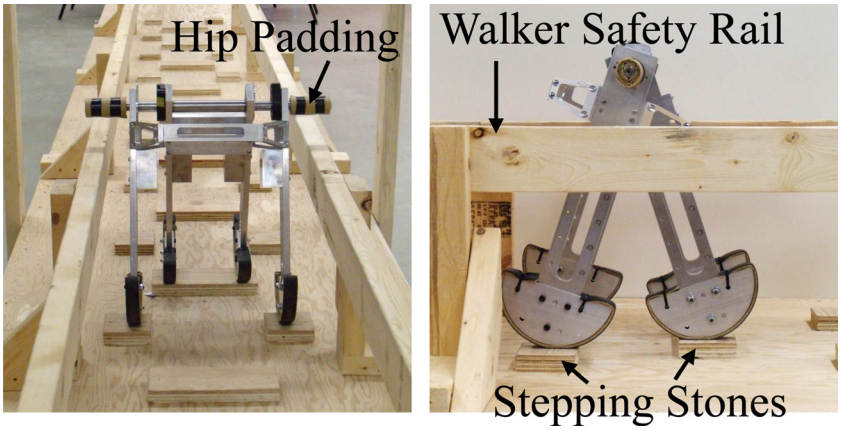

Fig. 8 Photos of HM2L on the ramp

Table 1 HM2L geometric parameters

Item	Symbol	Measurement
Walker height	l	40.64 cm
Walker width	w	30.61 cm
Foot radius[a]	P	8.13 cm

[a]With no sole.

Table 2 HM2L mass parameters

Item	Inside		Outside	
Mass (kg)	5.144	44.35%	5.172	44.59%
Hip mass (kg)	1.282			
Total mass (kg)	11.595			

Table 3 Variable HM2L parameters

	Center of mass[a] b		Radius of gyration[b] r_g	
Mass location	(m)	b/l	(m)	r_g/l
$L\#1$	0.1356	32.72%	0.1192	28.77%
$L\#2$	0.1547	37.34%	0.1112	27.03%
$L\#3$	0.1739	41.96%	0.1077	26.00%
$L\#4$	0.1930	46.58%	0.1067	25.75%
$L\#5$	0.2122	51.21%	0.1091	26.32%
$L\#6$	0.2313	55.83%	0.1146	27.65%

[a]Center of mass is measured from the hip joint and normalized with the leg length.
[b]Radius of gyration is with respect to the center of mass and normalized with the leg length.

walker. The data collected was captured with a Quanser Q8 data acquisition board connected to a PC. The data was saved with a Simulink program that uses features from QuaRC.[2] The measurements were taken at ~5 kHz sampling rate for all of the devices. The inclinometer generated a pulse width modulation signal at 125 Hz.

3.2 Experimental Procedure. For each experimental trial, the same procedure was followed. The feet are initially locked together to zero the encoders, thereby using $\alpha = 0$ as the initial inner leg angle reference. A successful run down the ramp was counted if the walker made it at least ten steps or halfway down the ramp. Once ten successful runs down the ramp were made, the trial was ended.

The aim of the experimental trials was to determine the effect of the center of mass on the gait. Six trials, labeled L#1 to L#6, with a center of mass ranging from 32.72% to 55.83% measured from the hip, were planned. The same effect will be simulated using the proposed model. The mathematical model is considered validated by matching the simulated and experimentally determined effects.

To capture a good representation of the gait of the experimental walker, the step period, step length, and average hip velocity were calculated from the data recorded. To calculate the step period, step length, and average hip velocity, the inner leg angle and time of each heel strike are required. Figure 9 shows a sample of experimental data of the inner leg angle and hip acceleration magnitude taken during a trial. The inner leg angle is determined from the difference between the two encoder measurements. The squares in Fig. 9 are the maximum measured acceleration caused by each heel strike. The step period can be calculated by the time difference between consecutive acceleration peaks. The step length is the distance between the foot contact points when both feet are on the ground. The step length for each step was calculated at the maximum measured acceleration.

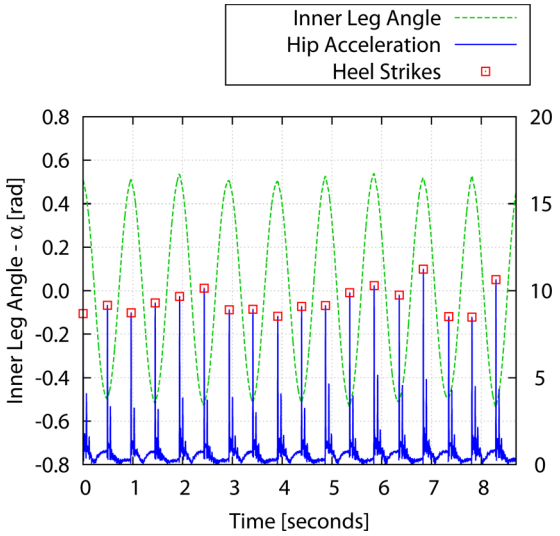

Fig. 9 Example of data from HM2L

When both feet are on the ground, the leg angles (with respect to the ramp normal) at the point of heel strike can be calculated using the measured inner leg angle (α) and Eqs. (20) and (21). When $\alpha > 0$, Eqs. (20) and (21) calculate the lead leg (ld) and trail leg (tr) angles, respectively. If $\delta = 0$, then $\theta_{ld} = \alpha/2$ and $\theta_{tr} = -\alpha/2$.

$$\theta_{ld} = \arctan\frac{l(1-\cos\alpha) + \rho(\cos(\alpha+\delta) - \cos\delta)}{l\sin\alpha + \rho(-\sin(\alpha+\delta) + \sin\delta)} \tag{20}$$

$$\theta_{tr} = \arctan\frac{l(1-\cos\alpha) + \rho(\cos(\alpha-\delta) - \cos\delta)}{-l\sin\alpha + \rho(-\sin(\alpha-\delta) + \sin\delta)} \tag{21}$$

Using the calculated leg angles, the step length when both feet are on the ground, L_{step}, can be calculated using Eq. (22).

$$L_{\text{step}} = (l\sin\theta_{ld} - \rho\sin(\theta_{ld} - \delta)) - (l\sin\theta_{tr} - \rho\sin(\theta_{tr} - \delta)) \tag{22}$$

The average hip velocity over one step was determined with a combination of the inner leg angle, step period, and the geometry of the walker. The average hip velocity, $\bar{v}_{\text{hip}}$, can be calculated using Eq. (23), where T_{step} is the step period, θ^0_{ld} is the angle of the lead leg at the start of the step, and θ^1_{tr} is the angle of the same leg at the end of the step.

$$\begin{aligned}\bar{v}_{\text{hip}} &= \frac{c_x^{\text{hip}^0} - c_x^{\text{hip}^1} + \rho\left(\theta^0_{ld} - \theta^1_{tr}\right)}{T_{\text{step}}} \\ &= \frac{\left(l\sin\theta^0_{ld} - \rho\sin\left(\theta^0_{ld} - \delta\right)\right) - \left(l\sin\theta^1_{tr} - \rho\sin\left(\theta^1_{tr} - \delta\right)\right) + \rho\left(\theta^0_{ld} - \theta^1_{tr}\right)}{T_{\text{step}}}\end{aligned} \tag{23}$$

[2]Software developed by Quanser.

Table 4 Mass and geometric parameters

Model parameters	
$l = 0.4143$ (m)	$\rho = 0.860$ (m)
$\delta = 0°$ (degrees)	$\gamma = 2.05°$ (degrees)
$m = 5.1587$ (kg)	$M = 1.2826$ (kg)
$b = 0.1930$ (m)	$r_g = 0.1067$ (m)

Table 5 Contact parameters

Contact parameters	
$\mu_s = 0.38$	$\mu_c = 0.30$
$k_s = 9.3920 \times 10^5 \left(\mathrm{N/m}^{3/2}\right)$	$k_d = 1.6879 \times 10^7 \left(\mathrm{N/m}^{5/2}\right)$
$\sigma_0 = 10^5 (\mathrm{N/m})$	$\sigma_1 = 2\sqrt{\sigma_0}\ (\mathrm{Ns/m})$
$v_s = 10^{-4} (\mathrm{m/s})$	$\alpha^0 = 10^o (\mathrm{degrees})$

After the trials were completed, the data was processed using a postprocessing program developed in Matlab. At least two steps were removed from the beginning and end of each run down the ramp. If the step length and step period had not settled after two steps, more steps were removed.

4 Results and Discussion

4.1 Repeatable Gait With Different Contact Models. The proposed mathematical model is able to capture additional gait features, like the double support phase, compared to the impact-based passive walking model. With the added complexity of the contact force and friction force model, a solution of a repeatable gait was still found with the proposed model. To demonstrate some of the advantages of the proposed model, simulations were conducted, with the parameters shown in Tables 4 and 5. For comparison, simulations of the traditional impact-based passive walking model were completed with model parameters of Table 4. The initial conditions of the proposed passive walking model, Eq. (24), and the impact-based passive walking model, Eq. (25), were selected so that the system was already in a repeatable gait.

Proposed Passive Walking Mathematical Model

$$Q_0 = \Big[0.000\ 0.4114\ 0.1399\ 0.0512\ 0.1708$$
$$0.0048\ 2.8056 - 0.4126\ 3.000 \times 10^{-6}\ 0.493 \times 10^{-6}\Big]^T \quad (24)$$

Impact-Based Passive Walking Mathematical Model

$$Q_0 = [0.2414 - 0.2414 - 1.7314 - 0.7318]^T \quad (25)$$

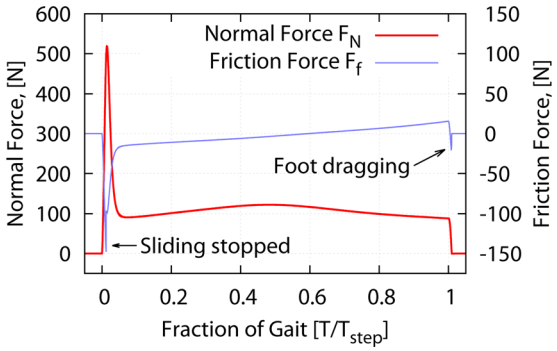

Fig. 11 Normal and friction force versus time

Fig. 10(*a*) shows the phase portrait of a leg angle versus leg angle velocity of the proposed model. The "impact" phase for the proposed model, shown in Fig. 10(*a*), was determined when the normal force of the impending stance leg just contacts the ground to when the normal force settles to near the steady state value of $(M + 2m)g$. The proposed model has a double support phase, shown with a thicker line in Fig. 10(*a*). Figure 10(*b*) shows the phase portrait of the leg angle of the impact-based model. The impact-based model heel strike regions are vertical, since the position state does not change over the impact. With the Hunt–Crossley 3contact model and the LuGre friction model, the position states of the proposed model change during the heels strike event, as they would in reality. As well, the contact and friction model allows the system to slide during the heels strike event (i.e., "no sliding during impact" condition is removed), if the tangential force is great enough to overcome the contact friction force. However, in the simulations conducted, the contacting foot only slid with a very low magnitude.

Figure 11 shows the normal force and friction force for one foot over one step. The initial peak in the normal force is due to the impact of the foot with the ramp. After the heel strike, the normal force settles to a value near the steady state normal force $(M + 2m)g$. The contact force still varies after the heel strike, due to the movement of the legs. During the heel strike, the friction force suddenly decreases when the foot stops sliding. The friction direction reverses twice throughout a single step. The second reversal is due to the foot dragging at lift off.

Figure 12 shows the friction state z for one leg over the swing and stance phases. Notice how the state observer is still active during the swing phase of the gait. Simulations were completed with resetting the state observer to zero after each separation, and no discernible difference was found between the resulting gaits.

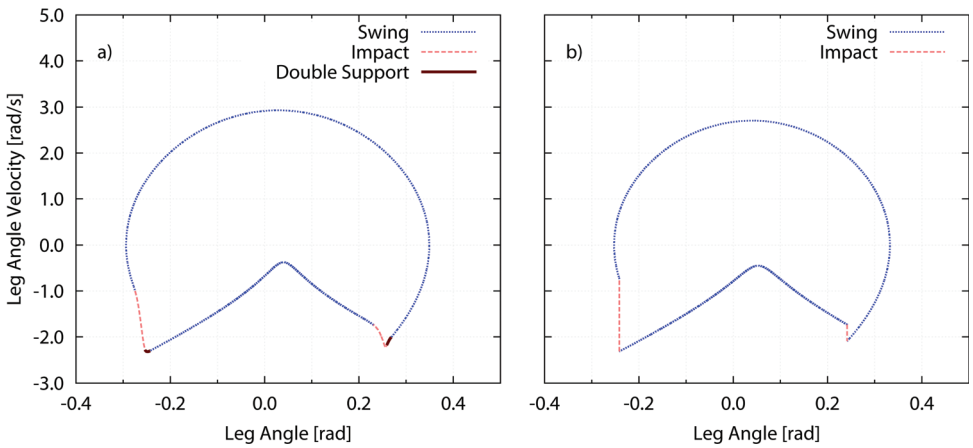

Fig. 10 Leg angle phase portrait. (*a*) Proposed model. (*b*) Impact-based model.

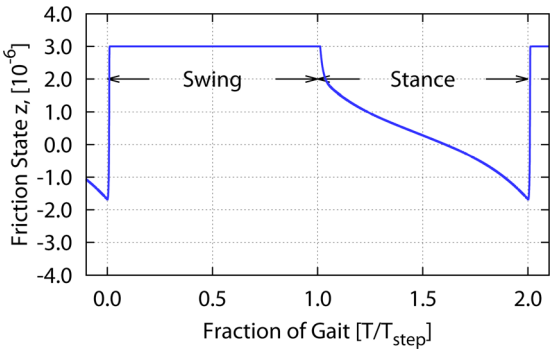

Fig. 12 Friction state observer

Table 6 Validation – geometric and mass parameters

Model parameters	
$l = 0.4143$ (m)	$\rho = 0.0860$ (m)
$\delta = 0°$ (degrees)	$\gamma = 2.05°$ (degrees)
$m = 5.1587$ (kg)	$M = 1.2826$ (kg)

Table 7 Validation – contact parameters

Contact parameters	
$\mu_s = 0.38$	$\mu_c = 0.30$
$k_s = 9.3920 \times 10^5 \left(\mathrm{N/m^{3/2}}\right)$	$k_d = 1.6879 \times 10^7 \left(\mathrm{N/m^{5/2}}\right)$
$\sigma_0 = 10^5 (\mathrm{N/m})$	$\sigma_1 = 2\sqrt{\sigma_0} (\mathrm{Ns/m})$
$v_s = 10^{-4} (\mathrm{m/s})$	$\alpha^0 = 10^o$ (degrees)

Table 8 Validation – variable parameters

	Center of mass b		Radius of gyration r_g	
Trial	(m)	b/l	(m)	r_g/l
L#1	0.1356	32.72%	0.1192	28.77%
L#2	0.1547	37.34%	0.1112	27.03%
L#3	0.1739	41.96%	0.1077	26.00%
L#4	0.1930	46.58%	0.1067	25.75%
L#5	0.2122	51.21%	0.1091	26.32%
L#6	0.2313	55.83%	0.1146	27.65%

Therefore, the equation for z was kept continuous throughout the whole simulation.

The sliding velocity between the ramp and the foot never stays at zero. However, the sliding velocity does remain below the Stribeck velocity. This may indicate that a friction model with the complexity of the LuGre model may not be needed to capture a majority of the dynamic features of the gait. A continuous friction model that accounts for transition between microsliding[3] and full sliding would be sufficient for this dynamic model.

4.2 Model Validation. In this section, the validation of the mathematical model is provided against experimental data gathered using the passive walker HM2L. As a reference, the impact-based passive walking model is compared against the experimental data as well. The effects of changing the center of mass on the step period, step length, and average hip velocity are used to compare the three resulting gaits of the experimental walker, proposed mathematical model, and impact-based model. The parameters used in the simulations for the validation case, rounded to four decimal spaces, can be found in Tables 6–8.

The geometric parameters were determined from the SolidWorks model that was used to generate the machine shop drawings for the passive walker HM2L. Each machined part, bolt, and nut of the walker was weighed, and the corresponding mass was entered in the SolidWorks model. Assuming a uniform density for each part, bolt, and nut, the mass properties of the walker were determined. To measure the angle of the ramp, a laser level was used to first measure the topography of the floor. Then, using the floor as a reference, the relative heights of four locations on the ramp were measured. Using the relative heights, the average angle of the ramp was determined.

The friction coefficients were estimated from measurements of a previous ramp and walker setup [30]. The parameters specific to the LuGre model (σ_0, σ_1, and v_s) were selected based on the information found in Ref. [31]. For the contact parameters, the steady state value of the deformation of the foot was measured when the walker was standing. Using the measured deflection and Eq. (26), the value of k_s was estimated. The contact damping parameter k_d was the only parameter that was used to adjust the model to fit the experimental data. Note that another way to estimate the contact

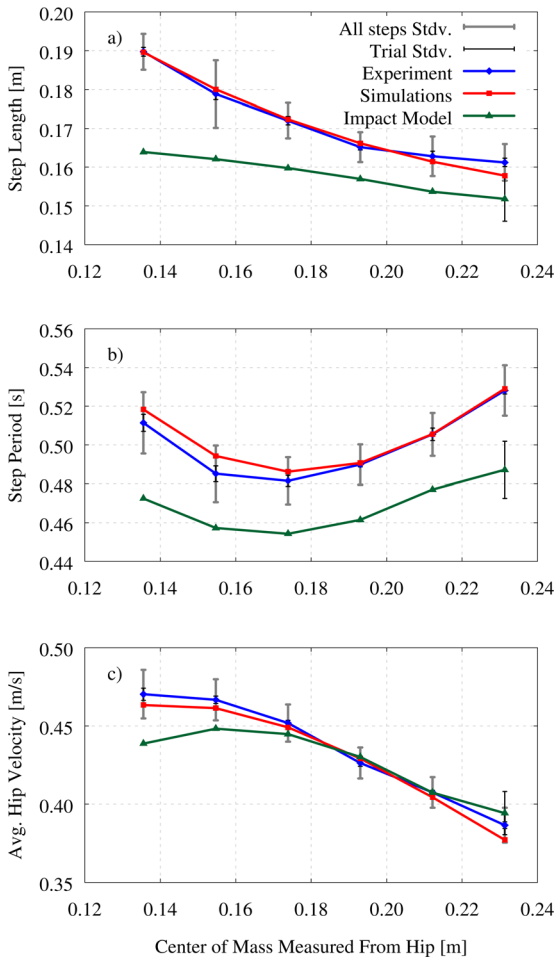

Fig. 13 Comparison between experimental walker, proposed model, and impact-based model. (*a*) Step length. (*b*) Step period. (*c*) Average hip velocity.

[3]The sliding velocity is less than the Stribeck velocity.

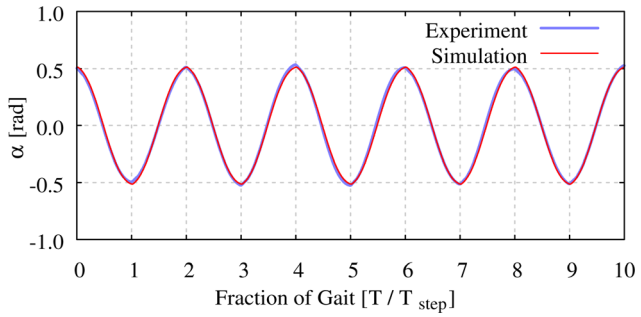

Fig. 14 Comparison of the inner leg angle (α) of the simulation and experimental gait

damping parameter is based on the mechanics of the contact process, as discussed in Ref. [32], where the parameter evaluation is based on the mechanics of the contact process. The parameter k_d was adjusted so that the experimental step length of trial CoM L#1 matched the simulations. The adjusted value of k_d was kept constant for the remaining simulations. For the simulations, only the center of mass and radius of gyration parameters were changed between trials to match the change of the parameters of the physical walker.

$$k_s = \frac{\left(\frac{1}{2}(2m+M)g\right)}{(h_{\text{measured}})^{\frac{3}{2}}} \tag{26}$$

Figure 13 shows the step length, step period, and average hip velocity for the proposed mathematical model, the impact-based model, and the experiments. The impact-based model was not stable at CoM L#6, but could take over 50 steps before falling. The unstable trial was treated similarly to the experiments, by taking an average of the steps completed and applying a standard deviation between the steps. The experiments have two sets of standard deviation bars. The "All steps Stdv." is the standard deviation between all of the usable steps of all of the runs down the ramp for that trial. The "Trial Stdv." is the standard deviation between the averages of each run down the ramp for that trial. The simulations of the proposed mathematical model match the experiment in both magnitude and trend. Thus, the ability of the proposed model to generate gait measurement trends is valid. The impact-based model matches the trends of the experiments, but not as closely as the proposed mathematical model. Although the impact-based model may be valid in some cases, Fig. 13 shows the inability of the impact-based model to replicate reality in this case.

To compare the kinematics of the experiments and simulations, the inner leg angle was compared. Figure 14 shows a comparison of the inner leg angle of the simulations and experiments for CoM L#4 from a single trial. Comparing the kinematics goes one step further than comparing the resulting gait measurements and shows how well the proposed model can match the physical walker's motion. The agreement between the inner leg angle of the physical walker and the proposed mathematical model shows that the proposed mathematical model can generate valid gait motion, not just valid gait measurement trends.

5 Conclusions

An advanced mathematical model of passive walking was developed with the Hunt–Crossley contact model and the LuGre friction model. Both the Hunt–Crossley contact model and the LuGre friction model are continuous and better represent the ground reaction forces. The proposed passive walking model was able to simulate the entire gait with one unified set of equations.[4] Even with the added complexity of the contact and friction models, repeatable periodic motion was produced. Furthermore, the proposed mathematical model was able to replicate the results of the experimental trials very well in both trend and magnitude. The conventional impact-based passive walking model can match the trends of the experimental gait, but was not able to match the magnitude of the gait parameters. The difference in magnitude between the two mathematical models is attributed to the proposed passive walking mathematical model being able to adjust the damping (i.e., energy loss) of the heel strike along with the ability to capture the necessary friction forces. The impact-based mathematical model was not stable for the same parameter range as the experiments and proposed mathematical model. The difference in stable parameter range is attributed to the effects of friction.

Overall, the proposed model has advantages over previous models in that (1) it captures more features and better represents the passive gait, due to the advanced contact and friction models, (2) the continuity of both contact and friction models avoids the theoretical problem of the solution concept for nonsmooth dynamic systems, as previous models encountered, and (3) the entire gait can be simulated with one unified set of equations, which avoids switching between equations, as the traditional impact-based model required. With the validated model, Part II provides a more in-depth analysis of the stability of the proposed passive walking model.

Acknowledgment

We acknowledge the funding from Natural Sciences and Engineering Research Council of Canada.

Appendix A

State Space Equations of Proposed Passive Walking Model. This section provides the detailed state space, Eq. (A1), for the proposed passive walking model

$$\dot{\boldsymbol{Q}} = f(\boldsymbol{Q}) \tag{A1}$$

$$\begin{aligned}\boldsymbol{Q} &= [Q_1\ Q_2\ Q_3\ Q_4\ Q_5\ Q_6\ Q_7\ Q_8\ Q_9\ Q_{10}]^T \\ &= \left[x_{\text{hip}}\ y_{\text{hip}}\ \theta_1\ \theta_2\ \dot{x}_{\text{hip}}\ \dot{y}_{\text{hip}}\ \dot{\theta}_1\ \dot{\theta}_2\ z_1\ z_2\right]\end{aligned} \tag{A2}$$

$$\begin{bmatrix}\dot{Q}_1\\ \dot{Q}_2\\ \dot{Q}_3\\ \dot{Q}_4\end{bmatrix} = \begin{bmatrix}Q_5\\ Q_6\\ Q_7\\ Q_8\end{bmatrix} \text{ and } \begin{bmatrix}\dot{Q}_5\\ \dot{Q}_6\\ \dot{Q}_7\\ \dot{Q}_8\end{bmatrix} = \boldsymbol{A}(\boldsymbol{Q})^{-1}\boldsymbol{B}(\boldsymbol{Q}) \tag{A3}$$

$$\dot{Q}_9 = v_1(\boldsymbol{Q}) - \sigma_0 \frac{|v_1(\boldsymbol{Q})|}{g_L(v_1(\boldsymbol{Q}))} Q_9 \tag{A4}$$

$$\dot{Q}_{10} = v_2(\boldsymbol{Q}) - \sigma_0 \frac{|v_2(\boldsymbol{Q})|}{g_L(v_2(\boldsymbol{Q}))} Q_{10} \tag{A5}$$

where Eqs. (A4) and (A5) are the state space form of the friction state observer equation, Eq. (15). The matrices $\boldsymbol{A}(\boldsymbol{Q})$ and $\boldsymbol{B}(\boldsymbol{Q})$ are defined by Eqs. (A6) and (A7).

$$\boldsymbol{A}(\boldsymbol{Q}) = \boldsymbol{M}(\boldsymbol{Q}) \tag{A6}$$

$$\boldsymbol{B}(\boldsymbol{Q}) = \boldsymbol{F}(\boldsymbol{Q}) - \boldsymbol{H}(\boldsymbol{Q}) - \boldsymbol{G}(\boldsymbol{Q}) \tag{A7}$$

where $\boldsymbol{M}(\boldsymbol{Q})$, $\boldsymbol{H}(\boldsymbol{Q})$, $\boldsymbol{G}(\boldsymbol{Q})$, and $\boldsymbol{F}(\boldsymbol{Q})$ are defined in Eqs. (3)–(6). The inverse of $\boldsymbol{A}(\boldsymbol{Q})$ was solved manually and simplified to the form shown in Eq. (A8).

[4]Does not switch between impact and motion equations like the traditional impact-based passive walking model.

$$\boldsymbol{A}(\boldsymbol{Q})^{-1}=\begin{bmatrix} \dfrac{A_M\left(c_1^2+c_2^2+A_M\right)+c_mc_p}{M_W} & \dfrac{A_{sc}(A_M+1)}{M_W} & -\dfrac{C_{AC}}{b} & -\dfrac{C_{CA}}{b} \\ \dfrac{A_{sc}(A_M+1)}{M_W} & \dfrac{A_M\left(s_1^2+s_2^2+A_M\right)-c_mc_p}{M_W} & -\dfrac{S_{AC}}{b} & -\dfrac{S_{CA}}{b} \\ -\dfrac{C_{AC}}{b} & -\dfrac{S_{AC}}{b} & \dfrac{A_MM_W}{b^2} & \dfrac{C_mM_W}{b^2} \\ -\dfrac{C_{CA}}{b} & -\dfrac{S_{CA}}{b} & \dfrac{C_mM_W}{b^2} & \dfrac{A_MM_W}{b^2} \end{bmatrix}\frac{1}{m\left(A_M^2-C_m^2\right)} \tag{A8}$$

$$c_1=\cos(\boldsymbol{Q}_3),\ c_2=\cos(\boldsymbol{Q}_4) \tag{A9}$$

$$s_1=\sin(\boldsymbol{Q}_3),\ s_2=\sin(\boldsymbol{Q}_4) \tag{A10}$$

$$M_W=2+\frac{M}{m} \tag{A11}$$

$$A_M=M_W\left(1+\left(\frac{r_g}{b}\right)^2\right)-1 \tag{A12}$$

$$A_{sc}=\sin(\boldsymbol{Q}_3)\cos(\boldsymbol{Q}_3)+\sin(\boldsymbol{Q}_4)\cos(\boldsymbol{Q}_4) \tag{A13}$$

$$C_m=\cos(\boldsymbol{Q}_3-\boldsymbol{Q}_4),\ S_m=\sin(\boldsymbol{Q}_3-\boldsymbol{Q}_4) \tag{A14}$$

$$C_p=\cos(\boldsymbol{Q}_3+\boldsymbol{Q}_4),\ S_p=\sin(\boldsymbol{Q}_3+\boldsymbol{Q}_4) \tag{A15}$$

$$C_{CA}=\cos(\boldsymbol{Q}_3)C_m+\cos(\boldsymbol{Q}_4)A_M \tag{A16}$$

$$S_{CA}=\sin(\boldsymbol{Q}_3)C_m+\sin(\boldsymbol{Q}_4)A_M \tag{A17}$$

$$C_{AC}=\cos(\boldsymbol{Q}_3)A_m+\cos(\boldsymbol{Q}_4)C_m \tag{A18}$$

$$S_{AC}=\sin(\boldsymbol{Q}_3)A_M+\sin(\boldsymbol{Q}_4)C_m \tag{A19}$$

$$\boldsymbol{B}(\boldsymbol{Q})=\begin{bmatrix} \left(F_{f_1}+F_{f_2}\right)+mb\left(\boldsymbol{Q}_7^2\sin\boldsymbol{Q}_3+\boldsymbol{Q}_8^2\sin\boldsymbol{Q}_4\right)+g(M+2m)\sin\gamma \\ \left(F_{N_1}+F_{N_2}\right)-mb\left(\boldsymbol{Q}_7^2\cos\boldsymbol{Q}_3+\boldsymbol{Q}_8^2\cos\boldsymbol{Q}_4\right)-g(M+2m)\cos\gamma \\ F_{f_1}c_{y_1}^{\text{hip}}+F_{N_1}c_{x_1}^{\text{hip}}-mgb\sin(\boldsymbol{Q}_3-\gamma) \\ F_{f_2}c_{y_2}^{\text{hip}}+F_{N_2}c_{x_2}^{\text{hip}}-mgb\sin(\boldsymbol{Q}_4-\gamma) \end{bmatrix} \tag{A20}$$

The normal force F_{N_i} is defined by Eq. (13). The friction force F_{f_i} is defined by Eq. (14). The contact positions relative to the hip, c_i^{hip}, are defined by Eq. (7).

Appendix B

Standard Impact Passive Walking Model. To compare the proposed mathematical model, a standard passive walking impact model was derived. The standard impact model derived in this section is similar to the impact-based passive walking models used by other researchers. The model developed in Ref. [6] assumed that $m << M$, so that the swing leg does not affect the stance leg, but the same assumptions are used for the impact equations that are used in this section. If $\rho=0$ and $\delta=0$, the impact model derived in this section simplifies to the model presented in Ref. [5]. The standard impact model has two parts: the equations of motion, Eq. (B1) and the impact transition equations, Eq. (B11). The subscript "*st*" refers to the stance leg, and the subscript "*sw*" refers to the swing leg.

$$\begin{bmatrix} M_{1,1} & M_{1,2} \\ M_{2,1} & M_{2,2} \end{bmatrix}\begin{bmatrix} \ddot{\theta}_{st} \\ \ddot{\theta}_{sw} \end{bmatrix}+\begin{bmatrix} H_{1,1} & H_{1,2} \\ H_{2,1} & 0 \end{bmatrix}\begin{bmatrix} \dot{\theta}_{st}^2 \\ \dot{\theta}_{sw}^2 \end{bmatrix}+\begin{bmatrix} G_1 \\ G_2 \end{bmatrix}=0 \tag{B1}$$

Note: In this section, $c=l-b$.

$$M_{1,1}=(m+M)l^2+m\left(c^2+r_g^2\right)+2\rho^2(2m+M)(1-\cos(\theta_{st}-\delta))+2\rho((m+M)l+mc)(\cos\theta_{st}-\cos\delta) \tag{B2}$$

$$M_{1,2}=-mlb\cos(\theta_{st}-\theta_{sw})+m\rho b(\cos(\theta_{st}-\theta_{sw}-\delta)-\cos\theta_{sw}) \tag{B3}$$

$$M_{2,1}=-mlb\cos(\theta_{st}-\theta_{sw})+m\rho b(\cos(\theta_{st}-\theta_{sw}-\delta)-\cos\theta_{sw}) \tag{B4}$$

$$M_{2,2}=m\left(b^2+r_g^2\right) \tag{B5}$$

$$H_{1,1}=\rho^2(2m+M)\sin(\theta_{st}-\delta)-\rho((m+M)l+mc)\sin\theta_{st} \tag{B6}$$

$$H_{1,2}=-mlb\sin(\theta_{st}-\theta_{sw})+m\rho b(\sin(\theta_{st}-\theta_{sw}-\delta)+\sin\theta_{sw}) \tag{B7}$$

$$H_{1,2}=mlb\sin(\theta_{st}-\theta_{sw})-m\rho b\sin(\theta_{st}-\theta_{sw}-\delta) \tag{B8}$$

$$G_1=g(-((m+M)l+mc)\sin(\theta_{st}-\gamma))+\rho((2m+M)(\sin(\theta_{st}-\delta-\gamma)+\sin\gamma)) \tag{B9}$$

$$G_2=gmb\sin(\theta_{sw}-\gamma) \tag{B10}$$

The impact transition equations are based on the assumption that angular momentum is conserved for the whole walker about the point of contact and for the stance leg about the hip. The postimpact angular velocities are determined by Eq. (B11), and the postimpact angular positions are determined by Eq. (B12), where the superscript "$_-$" denotes a state before the impact and "$_+$" denotes a state after the impact.

$$\begin{bmatrix} \boldsymbol{Q}_{1,1}^- & \boldsymbol{Q}_{1,2}^- \\ \boldsymbol{Q}_{2,1}^- & 0 \end{bmatrix}\begin{bmatrix} \dot{\theta}_{st}^- \\ \dot{\theta}_{sw}^- \end{bmatrix}=\begin{bmatrix} \boldsymbol{Q}_{1,1}^+ & \boldsymbol{Q}_{1,2}^+ \\ \boldsymbol{Q}_{2,1}^+ & \boldsymbol{Q}_{2,2}^+ \end{bmatrix}\begin{bmatrix} \dot{\theta}_{st}^+ \\ \dot{\theta}_{sw}^+ \end{bmatrix} \tag{B11}$$

$$\begin{bmatrix} 0 & 1 \\ 1 & 0 \end{bmatrix}\begin{bmatrix} \theta_{st}^- \\ \theta_{sw}^- \end{bmatrix}=\begin{bmatrix} \theta_{st}^+ \\ \theta_{sw}^+ \end{bmatrix} \tag{B12}$$

$$\boldsymbol{Q}_{1,1}^-=\rho^2(2m+M)(1-\cos(\theta_{st}-\delta)-\cos(\theta_{sw}-\delta)+\cos(\theta_{st}-\theta_{sw}))+\rho(((m+M)l+mc)(\cos\theta_{st}+\cos\theta_{sw}-\cos(\theta_{st}-\theta_{sw}-\delta)-\cos(\theta_{st}-\theta_{sw}+\delta))+mb(\cos\delta-\cos\theta_{st})) \tag{B13}$$

$$\boldsymbol{Q}_{1,2}^-=m\rho b(\cos\delta-\cos\theta_{sw})-mbc \tag{B14}$$

$$Q_{2,1}^{-} = m\rho b(\cos\delta - \cos\theta_{st}) - mbc \tag{B15}$$

$$\begin{aligned} Q_{1,1}^{+} = {} & 2\rho^2(2m+M)(1-\cos(\theta_{st}-\delta)) + \rho(2((m+M)l+mc) \\ & \times(\cos\theta_{st}-\cos\delta) + mb(\cos(\theta_{st}-\theta_{sw}-\delta)-\cos\theta_{sw})) \\ & +(m+M)l^2 + mc^2 - mlb\cos(\theta_{st}-\theta_{sw}) \end{aligned} \tag{B16}$$

$$Q_{1,2}^{+} = m\rho b(\cos(\theta_{st}-\theta_{sw}-\delta)-\cos\theta_{sw}) + mb^2 - mlb\cos(\theta_{st}-\theta_{sw}) \tag{B17}$$

$$Q_{2,1}^{+} = m\rho b(\cos(\theta_{st}-\theta_{sw}-\delta)-\cos\theta_{sw}) - mlb\cos(\theta_{st}-\theta_{sw}) \tag{B18}$$

$$Q_{2,2}^{+} = mb^2 \tag{B19}$$

To determine a numerical approximation to the impact model, ODE45 in Matlab was used to solve the equations of motion. The equations of motion are solved until the swing foot comes in contact with the ground. Then, the final state of the system is used as the preimpact state to calculate the postimpact state with Eqs. (B11) and (B12). The postimpact velocities and the final position of the walker are then used as the initial conditions for the next step, and the equations of motion are solved once again.

References

[1] Mochon, S., and McMahon, T. 1980, "Ballistic Walking: An Improved Model," Math. Biosci., **52**(3), pp. 241–260.

[2] McGeer, T., 1990, "Passive Dynamic Walking," Int. J. Robot. Res., **9**(2), pp. 62–82.

[3] McGeer, T., 1990, "Passive Walking With Knees," Proc. of the 1990 IEEE International Conference on Robotics and Automation, Cincinnati, OH, pp. 1640–1645.

[4] Goswami, A., Espiau, B., and Keramane, A., 1997, "Limit Cycles in a Passive Compass Gait Biped and Passivity-Mimicking Control Laws," Auton. Rob., **4**(3), pp. 273–286.

[5] Goswami, A., Thuilot, B., and Espiau, B., 1998, "A Study of the Passive Gait of a Compass Like Biped Robot: Symmetry and Chaos," Int. J. Robo. Res., **17**(12), pp. 1282–1301.

[6] Garcia, M., Chatterjee, A., Ruina, A., and Coleman, M., 1998, "The Simplest Walking Model: Stability, Complexity, and Scaling," ASME J. Biomech. Eng., **120**(2), pp. 281–288.

[7] Ikemata, Y., Yasuhara, K., Sano, A., and Fujimoto, H., 2008, "A Study of the Leg–Swing Motion of Passive Walking," Proc. of the 2008 IEEE International Conference on Robotics and Automation, Pasadena, CA, pp. 1588–1593.

[8] Borzova, E., and Hurmuzlu, Y., 2004, "Passively Walking Five-Link Robot," Automatica, **40**(4), pp. 621–629.

[9] Hurmuzlu, Y., and Chang, T.-H., 1992, "Rigid Body Collisions of a Special Class of Planar Kinematic Chains," IEEE Trans. Syst. Man Cybern., **2**(5), pp. 964–971.

[10] Mu, X., and Wu, Q., 2006, "On Impact Dynamics and Contact Events for Biped Robots Via Impact Effects," IEEE Trans. Syst. Man Cybern., Part B: Cybern., **36**(6), pp. 1364–1372.

[11] Wu, Q., Sekhavat, P., Sepehri, N., and Peles, S., 2005, "On Design of Continuous Lyapunov's Feedback Control," J. Franklin Inst., **342**(6), pp. 702–723.

[12] Gilardi, G., and Sharf, I., 2002, "Literature Survey of Contact Dynamics Modeling," Mech. Mach. Theory, **37**(10), pp. 1213–1239.

[13] Olsson, H., Åström, K., Canudas de Wit, C., Gäfvert, M., and Lischinsky, P., 1998, "Friction Models and Friction Compensation," Eur. J. Control, **4**(3), pp. 176–195. Available at: http://www.gipsa-lab.grenoble-inp.fr/~carlos.canudas-de-wit/publications/friction/dynamic_friction_EJC_98.pdf

[14] Boos, M., and McPhee, J., 2012, "Volumetric Modeling and Experimental Validation of Normal Contact Dynamic Forces," ASME J. Comput. Nonlinear Dyn., **8**(2), p. 021006.

[15] Qi, F., Wang, T., and Li, J., 2010, "The Elastic Contact Influences on Passive Walking Gaits," Robotica, **29**, pp. 787–796.

[16] Jafarian, M., 2010, "Variable Stiffness for Robust and Energy Efficient 2D Bipedal Locomotion," M.Sc. thesis, University of Twente, Enschede, Netherlands.

[17] Piiroinen, P., Dankowicz, H., and Nordmark, A., 2003, "Breaking Symmetries and Constraints: Transitions From 2D to 3D in Passive Walkers," Multibody Syst. Dyn., **10**, pp. 147–176.

[18] David, A., and Bruneau, O., 2011, "Bipedal Walking Gait Generation Based on the Sequential Method of Analytical Potential (SMAP)," Multibody Syst. Dyn., **26**, pp. 367–395.

[19] Font-Llagunes, J., Barjau, A., Pàmies-Vilà, R., and Kövecses, J., 2012, "Dynamic Analysis of Impact in Swing-Through Crutch Gait Using Impulsive and Continuous Contact Models," Multibody Syst. Dyn., **28**, pp. 257–282.

[20] Machado, M., Moreira, P., Flores, P., and Lankarani, H., 2012, "Compliant Contact Force Models in Multibody Dynamics: Evolution of the Hertz Contact Theory," Mech. Mach. Theory, **53**, pp. 99–121.

[21] Wu, Q., and Sabet, N., 2004, "An Experimental Study of Passive Dynamic Walking," Robotica, **22**, pp. 251–262.

[22] Wu, Q., and Chen, J., 2010, "Effects of Ramp Angle and Mass Distribution on Passive Dynamic Gait– An Experimental Study," Int. J. Human. Robot., **7**(1), pp. 55–72.

[23] Kazi, R., Koop, D., and Wu, C. Q., 2011, "Experimental Study on Passive Dynamic Bipedal Walking: Comparing Test Platforms and Effects of Parameter Changes on Gait Patterns," Proc. of the ASME 4th Annual Dynamic Systems and Control Conference, Arlington, VA.

[24] Ning, L., Junfeng, L., and Tianshu, W., 2009, "The Effects of Parameter Variation on the Gaits of Passive Walking Models: Simulations and Experiments," Robotica, **27**(4), pp. 511–528.

[25] Hunt, K., and Crossley, F., 1975, "Coefficient of Restitution Interpreted as Damping in Vibroimpact," J. Appl. Mech., **42**(2), pp. 440–445.

[26] Hertz, H., 2006, "On the Contact of Elastic Solids," *Miscellaneous Papers*, MacMillan, London, Chap. 5, pp. 146–162.

[27] Canudas de Wit, C., Olsson, H., Åström, K., and Lischinsky, P., 1995, "A New Model for Control Systems With Friction," IEEE Trans. Autom. Control, **40**(3), pp. 419–425.

[28] Flores, P., and Ambrósio, J., 2010, "On the Contact Detection for Contact-Impact Analysis in Multibody Systems," Multibody Syst. Dyn., **25**(1), pp. 103–122.

[29] Shampine, L., and Reichelt, M., 1997, The Matlab ODE Suite, MathWorks, Inc., Natick, MA.

[30] Koop, D., 2010, "Passive Dynamic Bipedal Walking: Ramp-Treadmill Comparison and Gait Variation Due to Parameter Change," B.Sc. thesis, University of Manitoba, Winnipeg, MB.

[31] Olsson, H., 1996, "Control Systems With Friction," Ph.D. thesis, Lund Institute of Technology, Lund, Sweden.

[32] Lankarani, H., and Nikravesh, P., 1994, "Continuous Contact Force Models for Impact Analysis in Multibody Systems," Nonlinear Dyn., **5**(2), pp. 193–207. Available at : http://link.springer.com/article/10.1007%2FBF00045676?LI=true#.